

# Auroral structure and dynamics from GOLD

Robert G Michell<sup>1</sup>

<sup>1</sup>NASA GSFC

November 26, 2022

## Abstract

The Global-scale Observations of the Limb and Disk (GOLD) mission data contain significant quantitative information about the aurora on a global scale. Here we present techniques for quantifying such information, including the temporal development of the structure within the auroral oval using the GOLD images. These techniques are applied to auroral observations in the GOLD data, in particular showing an example of how the longitudinal structure within the aurora varies over the course of six consecutive days with differing levels of geomagnetic activity. A simple model of the solar-induced airglow is presented that is used to remove the sunlight contamination from the dayside auroral observations. Comparisons to ground-based auroral imaging are used for the overall auroral context and to make estimates of the proportionality between the intensities of the green-line (557.7 nm) emission in the visible and the 135.6 nm emissions in the GOLD data. These observations are consistent with the intensity of the 135.6 nm auroral emission being on the same order as the intensity of the 557.7 nm auroral emission. They were both found to be around 1 kR for a stable auroral arc on a day with low geomagnetic activity (03 November 2018) and around 10 kR for an active auroral display on a day with higher levels of geomagnetic activity (05 November 2018). This could have important implications for making direct comparisons between space-based UV auroral imaging and ground-based visible-light auroral imaging and the total energy input estimates that are derived from them.

# 1 Auroral structure and dynamics from GOLD

R. G. Michell,<sup>1,2</sup>

---

R. G. Michell, University of Maryland, College Park, MD, USA

NASA Goddard Space Flight Center, Greenbelt, MD, USA. (robert.g.michell@nasa.gov)

<sup>1</sup>Department of Astronomy, University of  
Maryland, College Park, MD, USA

<sup>2</sup>NASA Goddard Space Flight Center,  
Greenbelt, MD, USA

2 **Abstract.** The Global-scale Observations of the Limb and Disk (GOLD)  
3 mission data contain significant quantitative information about the aurora  
4 on a global scale. Here we present techniques for quantifying such informa-  
5 tion, including the temporal development of the structure within the auro-  
6 ral oval using the GOLD images. These techniques are applied to auroral ob-  
7 servations in the GOLD data, in particular showing an example of how the  
8 longitudinal structure within the aurora varies over the course of six consec-  
9 utive days with differing levels of geomagnetic activity. A simple model of  
10 the solar-induced airglow is presented that is used to remove the sunlight con-  
11 tamination from the dayside auroral observations. Comparisons to ground-  
12 based auroral imaging are used for the overall auroral context and to make  
13 estimates of the proportionality between the intensities of the green-line (557.7  
14 nm) emission in the visible and the 135.6 nm emissions in the GOLD data.  
15 These observations are consistent with the intensity of the 135.6 nm auro-  
16 ral emission being on the same order as the intensity of the 557.7 nm auro-  
17 ral emission. They were both found to be around 1 kR for a stable auroral  
18 arc on a day with low geomagnetic activity (03 November 2018) and around  
19 10 kR for an active auroral display on a day with higher levels of geomag-  
20 netic activity (05 November 2018). This could have important implications  
21 for making direct comparisons between space-based UV auroral imaging and  
22 ground-based visible-light auroral imaging and the total energy input esti-  
23 mates that are derived from them.

## 1. Introduction

24 The Global-scale Observations of the Limb and Disk (GOLD) mission [*Eastes et al.*,  
25 2017] consists of an ultraviolet (UV) spectrograph on a geostationary satellite and thus can  
26 provide global scale images of Earth that contain the UV signatures of the aurora. When  
27 observing the aurora from space, the auroral emissions that occur in the far ultraviolet  
28 (FUV) part of the spectrum have certain advantages over those in the visible wavelengths.  
29 One of the main advantages of the far ultraviolet ( $\sim 130$  nm to  $\sim 190$  nm) is that the  
30 atmosphere efficiently absorbs these wavelengths and thus from a space-based vantage  
31 point, there is essentially no background of scattered light from the ground, as you would  
32 have when imaging in visible wavelengths. Thus making dayside and nightside auroral  
33 observations possible. However, this also means that these UV auroral emissions are  
34 completely unobservable from a ground-based vantage point. The atmospheric absorption  
35 of these FUV auroral emissions is also dependent on wavelength and thus (within the  
36 GOLD passband) the shorter wavelengths are more absorbed than the longer wavelengths.  
37 Therefore, it is possible to use the ratio of the intensities of the shorter wavelengths  
38 to the longer wavelengths (within the far ultraviolet band) to estimate the altitude at  
39 which the emissions are coming from and hence the characteristic (average) energy of  
40 the precipitating electrons [*Unick et al.*, 2016]. The total intensity of the aurora within  
41 these bands is considered to be proportional to the total electron flux [*Unick et al.*, 2016],  
42 however it is not as straightforward as it is with the 427.8 nm  $N_2^+$  emissions [*Rees and*  
43 *Luckey*, 1974] in the visible [*Murphree*, 1998].

44 Quantifying the total energy influx into the aurora and the average energy of the pre-  
45 cipitating electrons is fundamental to characterizing the aurora and its effects on the  
46 thermosphere, including ionospheric conductivity. Techniques for extracting these pa-  
47 rameters from UV imaging of the aurora have been described in the literature [*Strickland*  
48 *et al.*, 1983; *Lummerzheim et al.*, 1991; *Germany et al.*, 1997]. These techniques are sum-  
49 marized in *Germany et al.* [1997] where they describe a technique that uses the ratio of  
50 an LBH low band (centered around 150 nm) and an LBH high band (centered around 170  
51 nm) for inferring these fundamental auroral electron characteristics. The only significant  
52 excitation mechanism for the LBH emissions is electron impact ionization, therefore in the  
53 absence of photo-electrons, the LBH emissions act as a direct proxy for incident electron  
54 precipitation fluxes [*Germany et al.*, 1997]. The O<sub>2</sub> Schumann-Runge (S-R) absorption  
55 peaks within the FUV portion of the spectrum and decreases with longer wavelengths.  
56 Therefore if the incident electron energies are high enough to penetrate deep enough into  
57 the atmosphere, where there is a significant amount of O<sub>2</sub>, there will be differential absorp-  
58 tion as a function of wavelength. The shorter wavelengths (LBH-Low) will be absorbed  
59 more than the longer wavelengths (LBH-High) and therefore the ratio of these will vary  
60 significantly with increasing depth (decreasing altitude) hence with increasing average  
61 electron energy. Thus the ratio of the LBH-Low (with higher absorption due to O<sub>2</sub>) to  
62 the LBH-High (with less absorption due to O<sub>2</sub>) can be used as a proxy for the average  
63 electron energy. This ratio is calculated from 2 different emission bands from the same  
64 species and thus will be independent of any compositional changes that can occur, such  
65 as the significant changes in the O-to-N<sub>2</sub> ratio that can be associated with certain auroral  
66 activity. The LBH-High intensity can be used (in conjunction with simple transport mod-

67 eling) to estimate the incident total energy flux of electrons. Another important emission  
68 in the FUV is the 135.6 nm emission from atomic oxygen (OI).

69 Figure 1 shows a representation of the auroral spectrum in the FUV, showing the relative  
70 intensities of the main emission lines. The three main spectral regions of interest in the  
71 typical GOLD analyses (135.6 nm, LBH-Low and LBH-High) are denoted by the colored  
72 boxes. In Summary: the overall GOLD passband is 134 nm to 166 nm; the 135.6 nm  
73 band is the sum of the emissions between 133 nm and 137 nm; the LBH-Low band is the  
74 sum of the emissions between 140 nm and 148 nm and the LBH-High band is the sum of  
75 the emissions between 150 nm and 160 nm.

76 The main goal of this work is to demonstrate the usefulness of GOLD data, in particular  
77 the dayside GOLD observations, for quantifying the auroral structure and dynamics and  
78 to show that time-series of the auroral development over single days and many days can  
79 be created from these data. In addition, the nightside GOLD data can also be used to  
80 examine higher time resolution aspects of the auroral development over shorter timescales  
81 and without any solar contamination. An initial comparison is also made between the  
82 intensities of ground-based images in the visible (557.7 nm) and the space-based GOLD  
83 images in the FUV (135.6 nm).

## 2. Observations

84 The GOLD data contained in the available CDF files contain northern and southern  
85 hemisphere disk images across the whole GOLD passband and thus they can be summed  
86 into different wavelength bands of interest. The disk images of radiance are summed  
87 together into the appropriate wavelength bands (listed above and shown in Figure 1) in  
88 order to reproduce the disk images, such as those provided in the Level 1D summary plots,

89 where the aurora can clearly be identified. As a demonstration of the utility of the GOLD  
90 data for auroral observation, six consecutive days in early November 2018 were chosen for  
91 initial analysis. This time period was chosen because ground-based auroral observations  
92 taken from Poker Flat, AK were used to identify different levels of auroral activity and  
93 there were six days in a row (01 – 06 November 2018) that had clear visibility from Poker  
94 Flat, AK with varying levels of auroral activity. Initially, two days were examined, one  
95 day that had minimal auroral activity (03 November 2018) and another day (05 November  
96 2018) that had strong auroral activity. Figure 2 shows GOLD disk images (in 135.6 nm)  
97 of the northern hemisphere for these two separate nights in November 2018. These were  
98 taken in the dawn-sector and at the same local time each night (07:16 UT). The 135.6  
99 nm emission band was chosen for display because it has the brightest signal of the 3 main  
100 bands (as discussed above in Figure 1).

101 Figure 3 shows keograms that were constructed from the ground-based all-sky camera  
102 data (taken in the 557.7 nm band) by extracting a north-south intensity cut through  
103 an image every 5-seconds then subsequently stacking those lines into a 2-D array, with  
104 elevation angle of the field-of-view on the y-axis (corresponding to latitude) and time on  
105 the x-axis. This presentation allows for easily identifying the level of auroral activity and  
106 the latitude of the aurora throughout a given night. The black vertical line on Figure 3  
107 shows the time at which the two GOLD images were taken (07:15 UT) on both nights.

108 The aurora is clearly discernible in the GOLD images, even on the quiet auroral day,  
109 thus it is likely that the aurora will be visible in some form on nearly every day and night  
110 in the GOLD dataset. Therefore the GOLD auroral data can be used to study long-  
111 term seasonal and yearly variations in the auroral activity. The global view of GOLD

112 allows the longitudinal structuring to be quantified. In addition, the dayside GOLD  
113 data actually contain a time series of 32 disk images of each hemisphere, with an image  
114 every half hour, covering a time period of about 15.5 hours. These series begin in the  
115 dawn-sector, continuing through the noon-sector and into the dusk-sector. Therefore it  
116 is possible to quantify the temporal development of the longitudinal structuring. As a  
117 means to quantify the amount of longitudinal structuring and its temporal development,  
118 a type of keogram is constructed by taking an intensity slice through the auroral oval in  
119 the east-west direction (actually adding together several latitudinal rows of pixels inside  
120 the auroral oval) and subsequently stacking those into a new image. Figure 4 shows a  
121 panel of such keograms taken from the middle of the auroral oval for these two days (03  
122 and 05 November 2018) and over the three wavelength bands (135.6 nm, LBH-Low and  
123 LBH-High). In this representation, time is on the y-axis and longitude is on the x-axis.

124 There are several things to note from Figure 4. First, there are clear differences in  
125 auroral intensity and structuring between the day with more auroral activity (05 Nov)  
126 and the day with less auroral activity (03 Nov). Second, there are no significant differences  
127 in the structuring between the three wavelength bands, only differences in the intensity  
128 of the aurora. They are all plotted with the same intensity scale. Lastly, there is a clear  
129 contamination from the solar illumination (the diagonal bands through the middle of the  
130 keograms), when the aurora is in the daylight.

131 The nightside GOLD data do not suffer from solar contamination in the same way,  
132 however there are, in general, fewer images. Figure 5 shows the time series of aurora  
133 in nightside GOLD images (in the 135.6 nm band) from these two nights (03 and 05  
134 November 2018). These images are spaced 15 minutes apart, covering 45 minutes with

135 the four images. These represent all of the nightside images from these two days and it  
136 is clear that global longitudinal variations are seen, even on these relatively short time-  
137 scales. During the time of the dayside observations, 03 November had less auroral activity,  
138 by the night of 03 November turning into 04 November, the aurora had started to increase  
139 and was actually brighter than it was on 05 November at the same local time, however  
140 the aurora on 05 November still has a larger latitudinal extent. The GOLD nightside  
141 observations can be used to track the development of auroral features on shorter timescales  
142 (one-hour) and with an increased temporal resolution (15 minutes).

### 3. Discussion

143 The solar contamination present in the dayside GOLD auroral images presents a prob-  
144 lem when examining the dayside aurora, especially in the noon-sector. Figure 4 clearly  
145 shows that solar induced background is present in all wavelength bands and that it is  
146 time dependent. These bands of solar-induced airglow are often brighter than the auroral  
147 structures present at high latitudes. There is essentially no solar interference in the dawn-  
148 sector, before the terminator arrives and the dusk-sector, after the terminator passes, but  
149 the middle sunlit section is clearly contaminated by solar-induced airglow. Therefore in  
150 order to quantify the sunlit auroral structures, this time-dependent background signal  
151 needs to be removed. Luckily this signal is predictable and depends highly on the solar  
152 zenith angle (which is also included in the Geo-referenced GOLD data files). In an initial  
153 attempt to remove this signal, a simple model of this solar induced background was created  
154 that is proportional to the cosine of the solar zenith angle. Figure 6 (top) shows a portion  
155 of a disk image with the auroral region of interest highlighted by a white box. Keograms  
156 are constructed by taking an intensity slice through the middle of the box and stacking

157 them together to create the keogram. Figure 6 (bottom) shows a comparison between  
158 a keogram created from the raw intensity (left) and one created from the intensity with  
159 the solar contamination removed by subtracting off the simple model of the solar induced  
160 background (right). In this figure, the keograms are oriented so that time is on the x-axis  
161 and longitude is on the y-axis. The case with less active aurora (03 November 2018) was  
162 chosen because this would have a weaker auroral signal and if this can be extracted, then  
163 the brighter auroral signal on more active days would be clearly visible and quantifiable.

164 From Figure 6 it is clear that even such a simple model of the solar induced background  
165 removes most of the contamination, which reveals much more of the sunlit auroral features,  
166 including local time and longitudinal variations within the sunlit aurora. There is still  
167 some solar contamination, especially near the terminators, because the simple model  
168 used stopped at a solar zenith angle of 90 degrees, but in reality the solar induced airglow  
169 extends beyond that due to the finite thickness of the atmosphere. Future work will include  
170 a slightly more complicated model of the dayside airglow, as discussed in *Lummerzheim*  
171 *et al.* [1997]. In addition, it is possible that some of the dawn-dusk asymmetry in the  
172 keograms could be a result of the simplified method currently being used to create the  
173 keograms. Currently, a few horizontal rows of pixels are averaged together (the same  
174 pixels in each image) and these are then used to create the keogram. However, it is clear  
175 from the example disk image shown in the top of Figure 6 that the auroral oval is often  
176 tilted and thus a strictly horizontal cut will miss some of the aurora on either the dawn or  
177 the dusk side depending on which pixels are used to make the cut. For the data presented  
178 here, three rows of pixels are averaged together and they were chosen to be near the center  
179 of the auroral activity. This was done in order to minimize the amount of background

180 signal getting into the keograms. The same pixels were used for all the nights examined.  
181 In future analysis, a more clever approach will be used for creating the keograms, where  
182 a pixel mask will be used in order to just sample the pixels where the aurora occur.  
183 The auroral pixels will be determined by examining a larger number of auroral events,  
184 especially the more active events (which can be found using the ground-based auroral  
185 imaging data) so that the maximum extent of the aurora can be determined.

186 The continuous coverage of the dayside aurora provided by GOLD can be used to create  
187 long time-series of these longitudinal keograms (as presented in Figure 6). Applying  
188 the simple solar background removal algorithm to six consecutive days of GOLD data  
189 reveals that the structure and dynamics within the aurora can be captured and quantified.  
190 Figure 7 shows these six keograms (in two rows) on a continuous timescale from the 135.6  
191 nm band. These data cover 01–06 November 2018 and contain both quiet and active  
192 auroral conditions as well as the transitions between them.

193 This technique can be used to create a long time-series of the aurora, essentially over  
194 the life of the mission. There are gaps during the nightside in this representation, but  
195 using the available nightside data, some information could be added in. Even with just the  
196 dayside data, features of the overall auroral structure and dynamics can be quantified. For  
197 example, the aurora became active around the noon-sector on 04 November and stayed  
198 fairly active through 05 November, where the aurora became significantly brighter than  
199 the residual solar interference at the terminators, getting to a maximum brightness of  
200 around 15 kR on 04 November. On both of these active nights, the aurora showed a  
201 propagation from east to west starting in the noon-sector.

202 Figure 5 showed the GOLD nightside auroral images where 03 November 2018 (the  
203 quiet auroral day) showed brighter aurora than 05 November (the active auroral day).  
204 This long time-series keogram shows that the aurora at the end of 03 November (dusk)  
205 was beginning to intensify and was still intense on the beginning (dawn) of 04 November,  
206 while the aurora on the dusk side of 05 November was becoming less intense and was  
207 even less intense on the dawn-side of 06 November, which is consistent with the nightside  
208 images in Figure 5. This representation can be used to illustrate the overall behavior of  
209 certain aspects of the auroral oval over long periods of time.

210 The intensity of the aurora from the ground-based auroral imaging taken from Poker  
211 Flat, AK can be used to make general comparisons to the intensity of the aurora in the  
212 GOLD observations. The location of the aurora over Poker Flat, AK would however  
213 correspond to the extreme western side of the aurora visible in the GOLD images (near  
214 the limb). Thus it is not possible to make clear one-to-one comparisons of the auroral  
215 structures simultaneously visible in both data sets. However given that the overall struc-  
216 ture of the aurora is generally longitudinally extended, especially when features persist  
217 for several hours in either data set, it is likely that both GOLD and the ground-based  
218 imagers would observe similar features. Therefore a general comparison is made between  
219 the GOLD observations shown in Figure 2 and the ground-based auroral imaging shown  
220 in Figure 3. For 05 November 2018 (the active day), the intensity of the 135.6 nm emission  
221 is observed to be around 10 kR in the GOLD data at the extreme western edge of the  
222 auroral oval (closest to AK). At the same exact time, the ground-based auroral imaging  
223 observed the average intensity of the 557.7 nm emission to also be around 10 kR. Another  
224 point of comparison and perhaps a cleaner comparison can be made for the observations

225 on 03 November 2018 (the quiet day) because the aurora did not change much over many  
226 hours. Here the intensity of the 135.6 nm emission in the GOLD data on the extreme  
227 western edge of the auroral oval is around 1 kR. At the same time, the ground-based  
228 imaging (Figure 3) showed a quiet auroral arc in the north that lasted for more than 6  
229 hours and had an intensity of around 1 kR. These synergistic comparisons show that the  
230 intensities of the 135.6 nm emission and the 557.7 nm emission are on the same order.  
231 More quantitative comparisons can be made, using more days, in order to improve our  
232 estimate of the proportionality between these two emissions. Both the 135.6 nm emission  
233 and the 557.7 nm emission are from oxygen (OI) and thus it is possible that there is a  
234 clear proportionality between their intensities. This would be an important proportion-  
235 ality to understand because it would allow for better comparisons between ground-based  
236 and space-based auroral observations and could lead to improved estimates of auroral  
237 energy input on global scales.

#### 4. Conclusions

238 The GOLD disk images contain valuable information about the structure and dynamics  
239 of the aurora. The nightside GOLD data contain short time-series that can be used to ex-  
240 amine shorter timescale variations within the auroral oval, while the dayside observations  
241 can be used to create long time-series of auroral images and longitudinal keograms. Such  
242 keograms enable the quantification of the structure of the auroral oval and propagation  
243 of large-scale auroral features within it, especially those associated with active aurora,  
244 including substorms and the multi-day intensifications that result from magnetic storms.

245 The solar-induced airglow can be mostly removed from the sunlit auroral observations  
246 in the dayside GOLD data using a simple method. This method estimates the solar-

247 induced airglow intensity as being proportional to the cosine of the solar zenith angle and  
248 then subtracts this modeled background from the observed intensities. This works well  
249 to remove the majority of the solar contamination, but some interference remains near  
250 the terminators, due to the simplicity of the background model and the three-dimensional  
251 nature of the atmosphere. Even with such a simple model of the background, the sunlit  
252 auroral intensities can be observed above the background levels, even for moderate and  
253 weak auroral activity levels.

254 A synergistic comparison is made between the 135.6 nm band auroral intensity from  
255 the GOLD observation and the 557.7 nm auroral intensity observed from ground-based  
256 auroral imaging taken at Poker Flat, AK. Even though Poker Flat is not exactly within the  
257 field of view of the GOLD imager, the aurora at the extreme western edge of the auroral  
258 oval observed in the GOLD data would be fairly close to being over Alaska (within an  
259 hour of local time). Therefore, a comparison is made for the two nights examined in  
260 detail (03 and 05 November 2018) and similar intensities were observed in the 135.6 nm  
261 GOLD observations and the 557.7 nm ground-based observations. On 05 November (the  
262 more active day), the Gold observations showed the 135.6 nm aurora to be around 10 kR  
263 and the 557.7 nm aurora from the ground-based imaging was also observed to be around  
264 10 kR. On 03 November 2018 (the less active day), the 135.6 nm band was observed to  
265 be around 1 kR and the 557.7 nm band was also observed to be around 1 kR. This 1  
266 kR aurora in the 557.7 nm ground-based imaging data was stable and lasted for over 5  
267 hours centered around the time of the GOLD image. Therefore the ground-based imaging  
268 and GOLD would have measured the same auroral structure, making this an accurate  
269 comparison. These observations are consistent with the intensity of the 135.6 nm auroral

270 emission being on the same order as the intensity of the 557.7 nm auroral emission. This  
271 could have important implications for making direct comparisons between space-based  
272 UV auroral imaging and ground-based visible-light auroral imaging and the total energy  
273 input estimates that are derived from such observations.

274 **Acknowledgments.** This work was supported in part by National Science Founda-  
275 tion Grant AGS1523097. The GOLD data were provided courtesy of NASA/GOLD  
276 and the mission science team and are all freely available to the public at:  
277 <https://gold.cs.ucf.edu/data/>.

## References

- 278 Eastes, R. W., W. E. McClintock, A. G. Burns, D. N. Anderson, L. Andersson, M. Co-  
279 drescu, J. T. Correira, R. E. Daniell, S. L. England, J. S. Evans, J. Harvey, A. Krywonos,  
280 J. D. Lumpe, A. D. Richmond, D. W. Rusch, O. Siegmund, S. C. Solomon, D. J. Strick-  
281 land, T. N. Woods, A. Aksnes, S. A. Budzien, K. F. Dymond, F. G. Eparvier, C. R.  
282 Martinis, and J. Oberheide (2017), The Global-Scale Observations of the Limb and Disk  
283 (GOLD) Mission, *Space Sci. Rev.*, *212*(1-2), 383–408, doi:10.1007/s11214-017-0392-2.
- 284 Germany, G. A., G. K. Parks, M. Brittnacher, J. Cumnock, D. Lummerzheim, J. F.  
285 Spann, L. Chen, P. G. Richards, and F. J. Rich (1997), Remote determination of auroral  
286 energy characteristics during substorm activity, *Geophys. Res. Lett.*, *24*(8), 995–998,  
287 doi:10.1029/97GL00864.
- 288 Lummerzheim, D., M. H. Rees, J. D. Craven, and L. A. Frank (1991), Ionospheric con-  
289 ductances derived from DE-1 auroral images, *Journal of Atmospheric and Terrestrial*  
290 *Physics*, *53*, 281–292, doi:10.1016/0021-9169(91)90112-K.

- 291 Lummerzheim, D., M. Brittnacher, D. Evans, G. A. Germany, G. K. Parks, M. H. Rees,  
292 and J. F. Spann (1997), High time resolution study of the hemispheric power carried  
293 by energetic electrons into the ionosphere during the May 19/20,1996 auroral activity,  
294 *Geophys. Res. Lett.*, *24*(8), 987–990, doi:10.1029/96GL03828.
- 295 Murphree, J. (1998), Uv auroral imaging, in *Magnetospheric Research with Advanced*  
296 *Techniques, COSPAR Colloquia Series*, vol. 9, edited by R. Xu and A. Lui, pp. 51 – 59,  
297 Pergamon, doi:https://doi.org/10.1016/S0964-2749(98)80009-7.
- 298 Rees, M. H., and D. Luckey (1974), Auroral electron energy derived from ratio of spec-  
299 troscopic emissions. I - Model computations, *J. Geophys. Res.*, *79*, 5181–5186, doi:  
300 10.1029/JA079i034p05181.
- 301 Strickland, D. J., J. R. Jasperse, and J. A. Whallen (1983), Dependence of auroral FUV  
302 emissions on the incident electron spectrum and neutral atmosphere, *Journal of Geo-*  
303 *physical Research*, *88*(A10), 8051–8062, doi:10.1029/JA088iA10p08051.
- 304 Unick, C., E. Donovan, E. Spanswick, and V. Uritsky (2016), Selection of FUV auroral  
305 imagers for satellite missions, *Journal of Geophysical Research (Space Physics)*, *121*(10),  
306 10,019–10,031, doi:10.1002/2016JA022627.

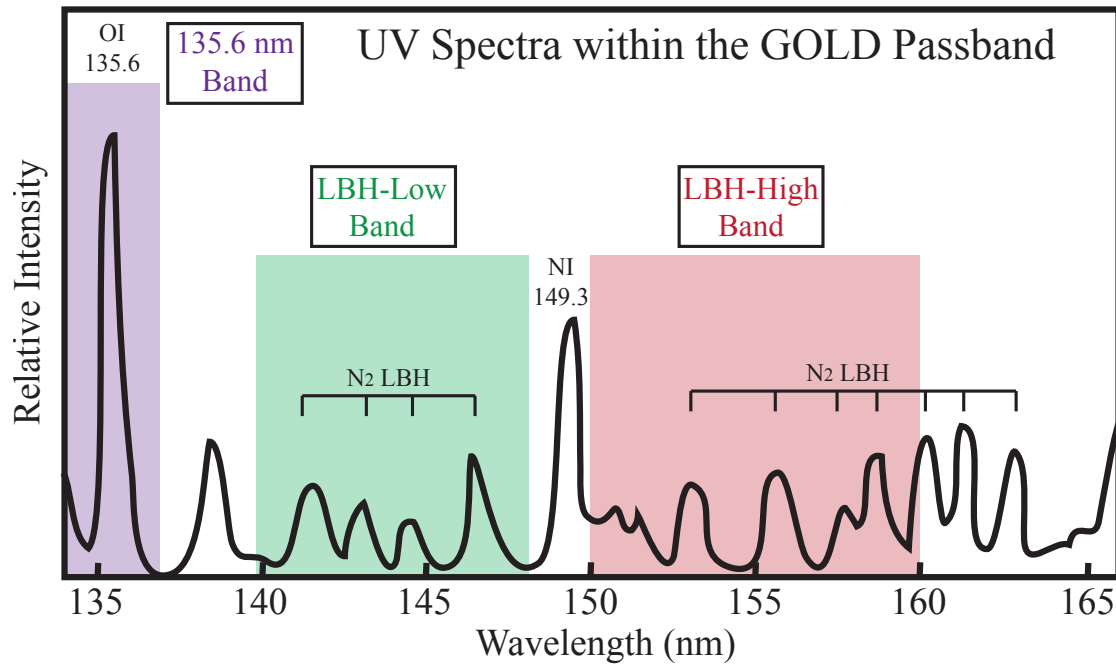
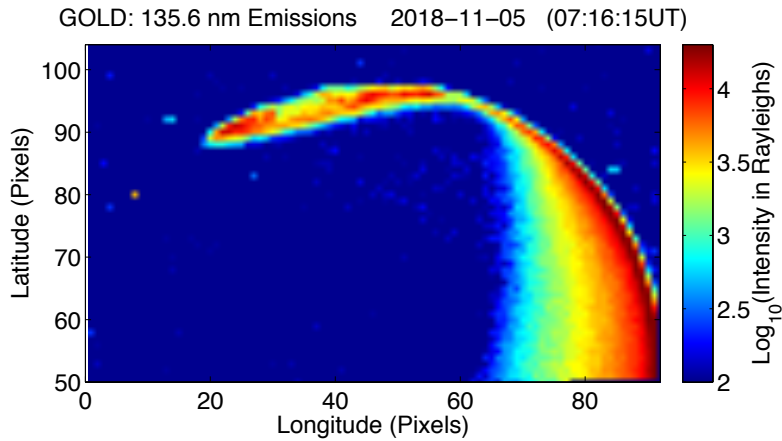


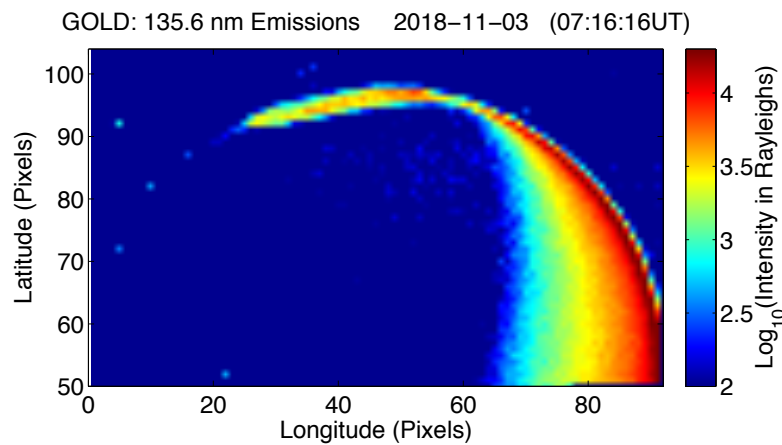
**Figure 1.** Representation of the FUV auroral spectra within the GOLD passband, showing the approximate relative intensities of the different auroral bands. The main spectral regions of interest that are defined in the GOLD data products guide are shown as the different colored boxes.

# Aurora from GOLD

## GOLD Image of Active Aurora: 05 Nov 2018

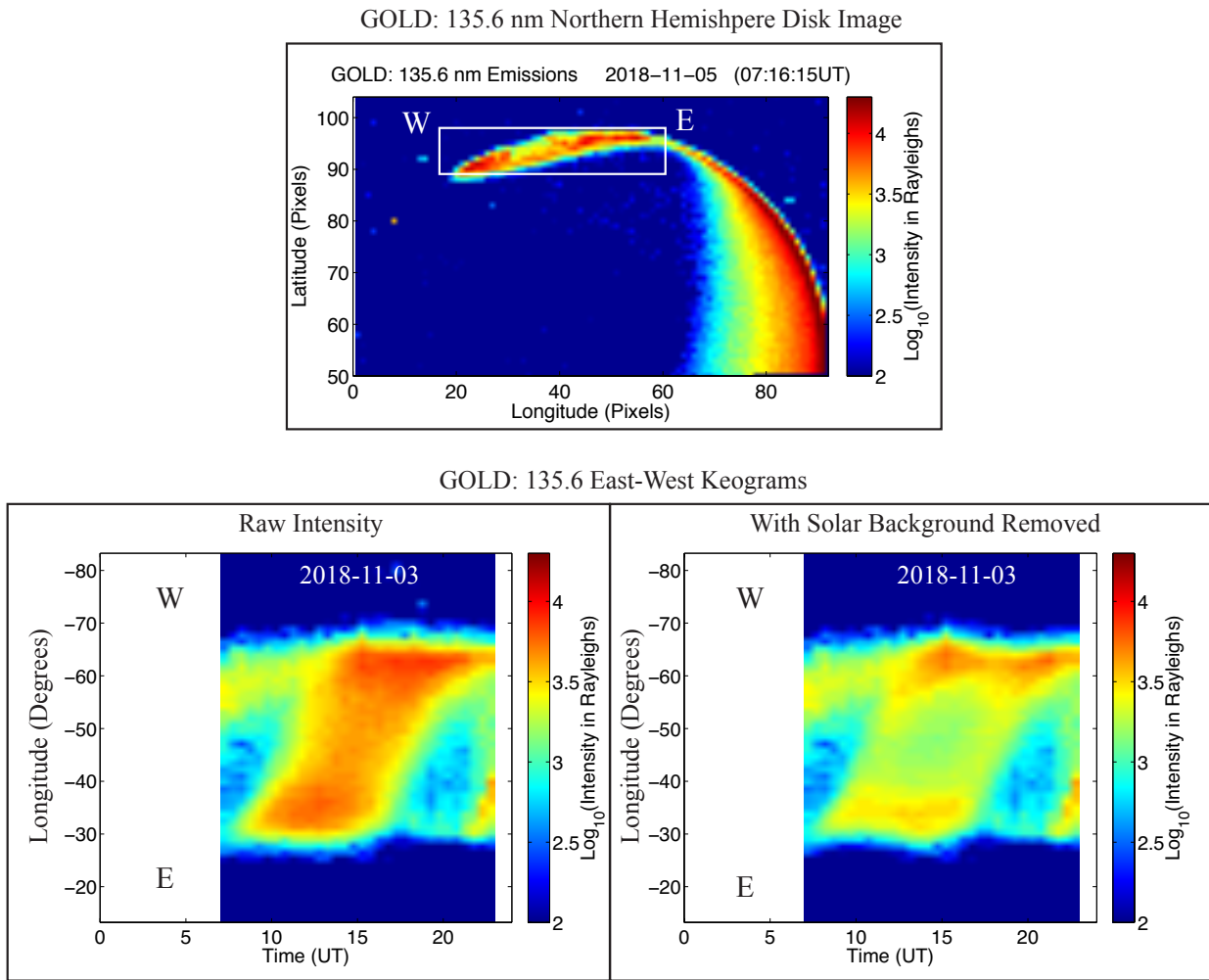


## GOLD Image of Quiet Aurora: 03 Nov 2018



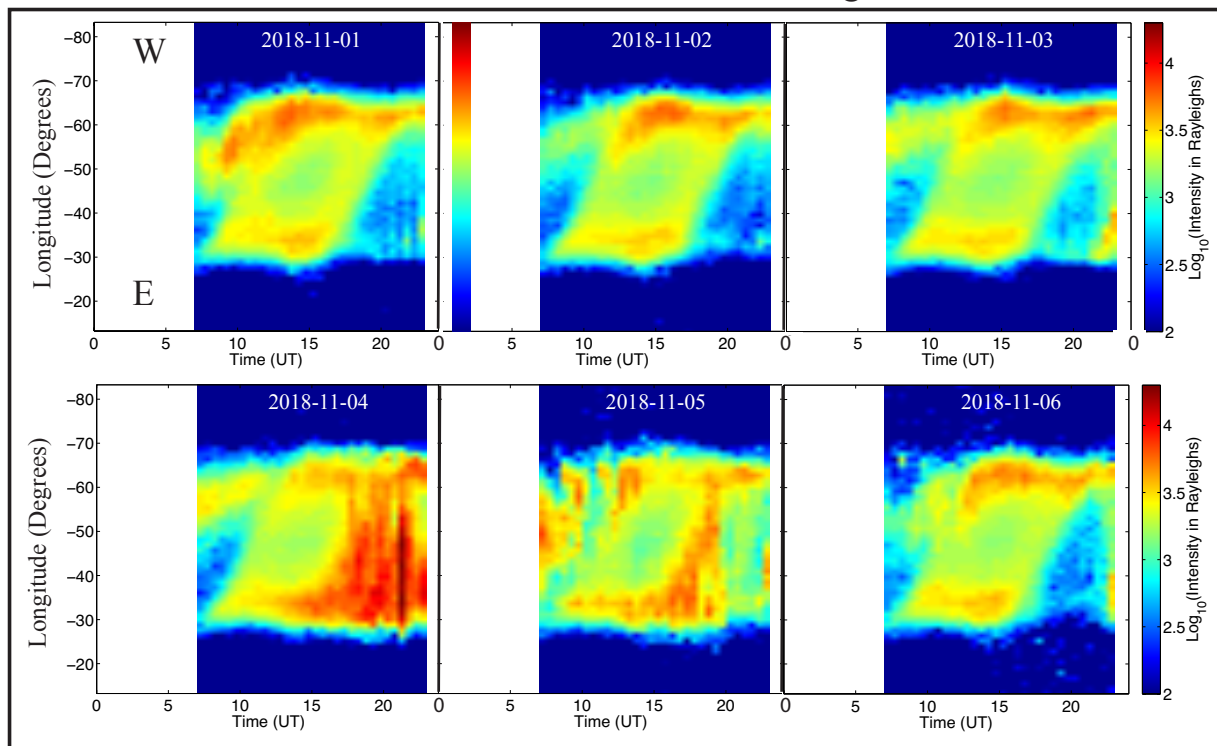
**Figure 2.** GOLD disk images (in the 135.6 nm band) of the northern hemisphere aurora, for an active night (05 Nov) and a quiet night (03 Nov) Both images are taken at the same local time (07:16 UT) in the dawn-sector.

Figure 3. Keograms of 557.7 nm visible-light aurora from Poker Flat, AK for the same two nights as the GOLD data presented in Figure 2 and displayed on the same intensity scale. The black vertical line represents the time when the GOLD images were taken.



**Figure 6.** GOLD disk image with the auroral region of interest highlighted by a white box (top). Comparison between a keogram created from the raw intensity (left) and one created from the intensity with the solar contamination removed by subtracting off the simple model of the solar induced background (right).

### GOLD: 135.6 nm East-West Keograms



**Figure 7.** Consecutive time-series of longitudinal keograms constructed from the 135.6 nm band dayside GOLD images of the aurora for six days (01–06 November 2018).